Slowly sheared dense granular flows: Crystallization and nonunique final states

J.-C. Tsai[1] and J. P. Gollub[2,*]
[1]*Department of Physics, Haverford College, Haverford, Pennsylvania 19041, USA*
[2]*Department of Physics and Astronomy, University of Pennsylvania, Philadelphia, Pennsylvania 19104, USA*
(Received 2 April 2004; published 21 September 2004)

Simultaneous time-resolved measurements of internal structure, granular volume, and boundary shear force are reported for dense granular packing steadily sheared under a fixed normal load. We identify features of the crystallization transition for a deep shear flow, whose height-dependent local mean velocity spans more than five orders of magnitude. This structural change is accompanied by a significant decrease of granular volume and shear force, with a more rapid falloff of particle velocity with depth than occurs in the disordered state. Boundary conditions can have a profound influence on the crystallization of the entire packing. We find that continuously sheared flow can exhibit nonunique final states even under identical boundary conditions; a few cycles of oscillatory pretreatment can initiate states that evolve into either a crystallized or a disordered final state after long-term unidirectional shearing. On the other hand, the disordered state can be stabilized after being sufficiently compacted by unidirectional shear. These experiments raise interesting questions about how prior history is recorded in the internal structure of granular packings, affecting their instantaneous rheology and long-term evolution in response to shear.

DOI: 10.1103/PhysRevE.70.031303 PACS number(s): 83.80.Fg, 45.70.Mg, 83.10.Tv, 83.50.Ax

I. INTRODUCTION

Granular flow is noteworthy both for the range of surprising phenomena it exhibits, and for the challenge it has provided to theoretical explanation [1–4]. Several distinct regimes have been identified. One extreme case is the rapid-flow regime: the dynamics of rapid flow is often described using the framework of dissipative kinetic theory with flowing grains bearing some resemblance to molecules in a gas. On the other hand, when particles do not have sufficient relative speed to sustain the pressure exerted by their neighbors, they tend to collapse into a dense creeping state in which particles roll or slide over each other. Creeping can be either localized or global depending on the circumstances. For example, it can be local in industrial blenders [5,6], or global in some extremely slow flows in geological settings [7]. It is also known that changing the stress level in a sheared large-scale granular packing can qualitatively alter its velocity profile as a result of differences in the contact network, even though the corresponding fractional deformations of individual grains are all very small [8]. Furthermore, the state of the flow in the slowly creeping regime can exhibit significant change over time.

Despite the wealth of observed phenomena, the theory for slow flows of densely packed granular materials is less developed than the theory of rapid flows. Approaches using kinetic theory may be of limited value here. For instance, it is tempting to suppose that the elastic energy stored between grain contacts is negligible in comparison to the kinetic energy for particles as rigid as glass. However, it has been estimated [9] that for millimeter-sized glass beads moving at a relative speed of several bead diameters per second under the static pressure of a layer of material that is several centimeters thick, the mean kinetic energy is actually smaller than the average elastic energy, and may be the least important quantity in accounting for the creeping dynamics. Recent theories show that the elasticity of grains can often play a vital role in the rheology of dense granular flows [10]. A number of analytic theories and models involving frictional interaction and plasticity have been attempted [11–17], while some of the assumed constitutive relations can be hard to verify on a microscopic level. Experimentally, monitoring dense granular packings driven by continuous boundary shear is a useful way to study the evolution of creeping flow; an apparently steady state can gradually undergo substantial change or, in some cases, make sharp transitions as we report in this work.

The connection between the internal structure of the material and the rheology of flow turns out to be particularly interesting. Here we sample a few previous investigations regarding shear-induced ordering in systems not limited to granular flows. Shear-induced ordering has been observed in computer simulations of uniformly sheared particle suspensions, in which the fluid-mediated hydrodynamic interactions between particles govern the dynamics [18]; these computations do not impose a thermostat as might be done in other simulations intended for systems of smaller particles with prominent Brownian motions. In computer simulations of particles uniformly sheared under the influence of theoretical thermostats [19–23], some intrinsic time scales controlled by the imposed temperature can be defined, such as the mean diffusion time or thermal collision interval; the observed ordering behavior often depends on the rate of the macroscopic shear. The simulations of sheared particles with repulsive interactions (mimicking the behavior of dilute charged colloidal particles [24]) suggest that the presence of a shear velocity field can either enhance or suppress particle ordering [21,22]. However, the proper interpretation of the ordering in these simulations with artificial thermostats is apparently still controversial, as is pointed out in Ref. [23], due to some

*Electronic address: jgollub@haverford.edu

difficulties in connecting these computations to specific experimental conditions. In experiments of uniformly sheared colloidal suspensions, researchers have demonstrated that particles can exhibit ordering that leads to significant change of rheology, e.g., in Refs. [25,26].

In the case of slowly creeping millimeter-sized granular particles, the contact forces between densely packed grains dominate the dynamics; there are no obvious intrinsic time scales analogous to, for example, those related to either interactions with interstitial fluids or thermal motions that are controlled by the thermostat. In addition, the velocity of grains often spans many orders of magnitude in a macroscopic sheared granular packing; the characteristic time for local relative displacement between grains, defined by the inverse of the local velocity gradient, exhibits a wide spectrum. Some interesting questions arise: Can a sheared granular packing exhibit spatial order in the presence of such a strong inhomogeneity in space? How does the internal order impact the rheology of granular flow? Experimentalists have observed ordering of granular spheres when grains are poured into vibrating containers with suitable boundary conditions [27,28]. Recent soft sphere simulations of a large-scale gravity-driven granular flow [29] also find intermittent crystallization on an ordered substrate. However, existing theories of densely packed granular flows [11–17] generally have not included the effect of spatial order, partly because of the scarcity of experimental information about the internal structure of steadily flowing granular particles.

Experimentalists have investigated the phenomena of slowly creeping granular materials from various points of view. Observations by Komatsu *et al.* [30] on particles in a thick but quasi-two-dimensional (2D) pile of flowing sand imply that the velocity of creeping grains can extend far from the surface into the deep bulk, spanning several orders of magnitude. Behringer and co-workers [31] measure the local contact forces at the lower boundary of a slowly sheared dense granular packing: the fluctuation spectrum (with frequencies scaled by the boundary driving velocity) of local contact forces is invariant over a wide range of driving speeds. This observation illustrates the quasistatic nature of the creeping flow, i.e., the grains are almost always in static equilibrium. Mueth *et al.* [32] use a magnetic resonance imaging (MRI) technique to study particles in a sheared layer several grain diameters thick, and determine the velocity field of the internal mass flow with sub-grain-size spatial resolution; they have pointed out the effect of particle layering on the mass flow field. In addition, the fluctuating motion of granular particles at the bottom of a Coutte shear cell [33], or at its upper surface [34], has been measured; the relation between the local velocity gradient and the fluctuating components of grain motion has been studied in depth.

The goal of the present work is to investigate the time evolution of sheared granular flows in the creeping regime, and to elucidate the connection between internal structure and granular rheology. Our model system contains glass particles in an annular channel; the granular material is subjected to a fixed vertical load and sheared from above at a constant speed. Simultaneous measurements of internal particle structure, granular volume, and boundary shear force are performed as the granular packing evolves over time; a novel internal imaging technique utilizes an interstitial fluid to index match the glass beads. We first focus on spherical particles of uniform size. More generally, polydispersity would introduce another factor affecting the evolution of the packing; a movie demonstrating the shear-induced segregation of a mixture of particles of different sizes in our system is available online.[1] The scope of the present work is to understand the intrinsic behavior by studying a nearly monodisperse system, as an initial step of exploring the evolution of granular creeping flows.

A number of papers on granular shear flows in the same geometry as in our work are reported in the literature. In addition to the local contact force measurements already cited [31], there are other experiments using low normal load and high shear rates: the relation between shear force and shear rate [35,36], as well as the granular self-diffusion as seen from the sidewall [37], has been the focus of these shear flows that are fully or partly in the regime of rapid-flow dynamics. It should be pointed out that the stress level and shearing speed in our experiments ensure that the entire packing is flowing in the creeping regime. In the Appendix, we estimate the range of driving speed that produces a globally creeping flow. In addition, some previous works in the same geometry focus on stick-slip behavior [38], whereas we impose a stationary driving in the measurements of velocity fields. However, one of the main phenomena, i.e., the crystallization transition to be reported in the following sections, actually does not require stationary driving.

Also, we create flow conditions with a hierarchy of forces in which the typical contact force between grains is much larger than the weight of one grain, which is in turn much greater than the maximal drag force provided by interstitial fluid. Therefore, the presence of fluid for imaging purposes in this work does not play a significant role in the creeping dynamics, except by reducing the apparent friction through lubrication.

II. EXPERIMENTAL METHODS

A. Main apparatus

The main apparatus is an annular channel formed by two concentric stationary glass cylinders, which are smooth and transparent (Fig. 1). We typically use spherical soda lime glass beads (density $\approx 2.5\ g/\mathrm{cm}^3$, elastic modulus ≈ 63 GPa, refractive index ≈ 1.54, from Jaygo, Inc.) of mean diameter $d = 0.68$ mm with a standard deviation 4% to fill the channel; the filling height is adjustable from a few particle diameters to $50d$. The distance between the inner and the outer walls is about $30d$ and the circumference is about $800d$. Fluid can be added to the interparticle space when internal imaging (described below) is planned. The glass beads are driven by a rotating ring-shaped upper boundary to which a monolayer of glass beads has been glued; the glued glass beads are packed at about the maximal area density and form local hexagonal structures with dislocations. Three different bottom boundary conditions are available: (1) flat bottom–

[1] http://www.haverford.edu/physics-astro/gollub/internal_imaging

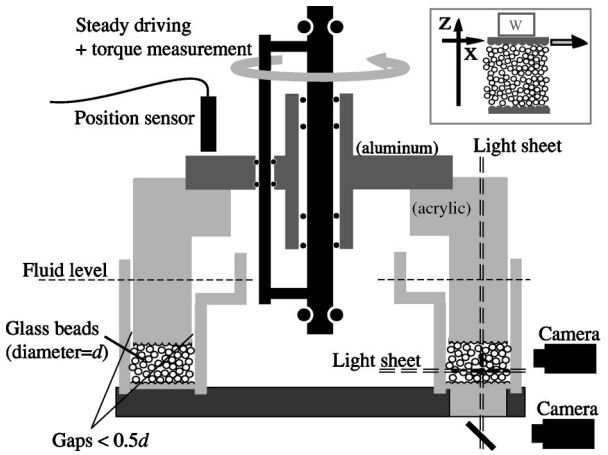

FIG. 1. Cross section of the annular channel filled with glass beads, with the inset showing a schematic side view and the definition of coordinates being used in this work. The shear and normal loads W are transmitted through a monolayer of glass beads glued to the rotating aluminum-acrylic assembly that is free to move vertically while maintaining constant rotation rate. Three different bottom conditions are available: flat, monolayer, and bumpy. Volume change is determined by detecting the vertical displacement of the upper assembly. The torque required to maintain the rotation is measured by a force gauge coupled to the motor through a pulling wire (not shown). Both vertical and horizontal slices of internal fluorescent images can be captured by digital cameras.

smooth acrylic; (2) monolayer bottom (described above); and (3) bumpy bottom–a mixture of 0.6- and 1.0-mm glass beads glued at approximately equal area fraction. In addition, a transparent window (thick polycarbonate) is made at the bottom of one part of the channel. The top surface of the acrylic part of the rotating assembly is also polished, to provide an option for viewing from the top.

The upper boundary is attached to a precision bearing that allows free but strictly vertical movement while rotating. The weight of the upper boundary assembly W provides a constant normal load of $(1.3\ \mathrm{kg})g$, which is about 12 times the total effective weight of the grains at the typical filling height of $24d$. (The buoyancy effect caused by the fluid has been accounted for the normal load and effective grain weight here.) Extra precision is demanded during the assembly process to ensure that the two planes defined by the upper and lower boundaries are parallel, and that the gaps between the upper boundary and the cylindrical walls are smaller than $0.5d$ around the circumference at all times, while the upper boundary rotates. The small gaps, combined with a fluid reservoir at the upper edge of the inner wall, allow the interstitial gas or fluid to exit or re-enter the channel freely, while the granular particles cannot escape. This allows the determination of the granular volume change by monitoring the height of the upper assembly. In practice, the height is measured once per rotation by detecting the position of a horizontal metallic arm installed on the rotating assembly and extending beyond the outer radius of the channel. An inductive-capacitive sensor is used for this purpose. (The design of the extended arm enables us to avoid calibration errors when the sensor is displaced, e.g., when changing particles.)

The unidirectional rotation is driven by a stepping motor (DM-4001 by Aerotech, Inc.) whose rotating shaft is rigidly connected to and aligned with the central shaft of our apparatus; the central shaft rotates with the same angular speed of the upper boundary, as shown on the figure. The combination of the microstepper of the motor and a $100\times$ speed reduction gear box gives an angular resolution of 2.5×10^{-5} rotations. Extra care is taken to maximize the rigidity of the driving mechanism. The deviation of motion of the upper boundary from an ideal constant-speed translation is less than $0.1d$; this is estimated by monitoring the projection (onto a distant screen) of a laser beam reflected from a mirror installed on the central shaft of our apparatus.

The shear force at the upper boundary can be determined if one measures the torque transmitted from the motor to the upper boundary or, alternatively, the torque that is required to resist the motor's tendency to rotate in the opposite direction. This is achieved by letting the motor stand freely on its own rotating shaft, decoupling it from its usual rigid support, attaching a pulling wire off center, and measuring the tension in the wire with a force gauge (PCB Piezotronics: KT-1102-01). However, the flexibility introduced by the pulling wire inevitably causes some unsteadiness in the upper boundary motion, so the motor is rigidly supported when the velocity profile is measured.

B. Internal imaging and image analysis

To image the interior, the interparticle space is filled with a special hydrocarbon mixture (viscosity ≈10 cS, density $\approx1\ g/\mathrm{cm}^{-3}$, from Cargille Laboratories). The refractive index of the fluid is fine-tuned to match that of the beads by adjusting the relative concentration of the ingredients to the accuracy of 10^{-3}. The optimal index-matching condition is determined by minimizing the scattering near the forward direction while a green He-Ne laser beam (543.5 nm) is sent though a test cell containing the mixture of beads and fluid. In gluing beads to the upper or lower boundary, adhesive (Norland NOA-68) with the closest refractive index to that of the glass beads is chosen and bubbles are avoided, in order to minimize the distortion of the image or the illuminating light sheet (described below) through these roughened boundaries.

A minimal amount of fluorescent dye (Exton Pyrromethene-580, fluorescent peak ≈540 nm) is blended into the fluid. A thin laser sheet enters the imaging region through either the bottom window or the front wall, to activate the fluorescence of the dye and create an instantaneous 2D image slice $\mathcal{I}_{slice}(\vec{x},t)$ in which particles appear as shadows. The image can be captured by digital camera through either the front wall or the bottom window. To create the laser sheet, a narrow beam from the 514.5nm line of an argon ion laser (Lexel-75) is first expanded isotropically (by a microscope objective), collimated (by a convex lens), and compressed one-dimensionally by a set of cylindrical lenses (including a pair of convex and concave lenses to create a tunable effective focal length $f\sim-2$ m, and a convex lens with $f=-6$ mm, located between the focal point of the tunable lens pair and our imaging area). The resulting laser sheet is narrower than $0.5d$ throughout the region of interest.

The fluorescent images are filtered with a cutoff wavelength 550 nm before reaching the camera, to screen out the undesired noise due to scattering of the excitation light.

To track the particles, an image is first converted to a 2D map $\mathcal{M}$ using a convolution

$$\mathcal{M}(\vec{x},t) = \int G'(|\vec{x}-\vec{x}'|) \cdot \mathcal{I}_{slice}(\vec{x}',t) \cdot d^2\vec{x}', \qquad (1)$$

in which $G'(r)$ stands for the derivative of a Gaussian ring

$$G'(r) = \frac{d}{dr} e^{-(r-a_0)^2/2\sigma_0^2} \qquad (2)$$

with radius a_0 being approximately the apparent radius of a particle in the image (from 9 to a few tens of pixels, depending on the image magnification), and the width σ being one or a few pixels. In practice, the convolution takes advantage of fast Fourier transform (FFT) techniques for the sake of computational efficiency. [39] The bright peaks in each map $\mathcal{M}$ represent the centers of particles in that frame, and can be found using previously developed computer routines [40] which also reconstruct particle trajectories from a set of sequential images. This convolution method is based on the idea of edge recognition (similar to Hough transformation [41]), and therefore can still resolve particles in the presence of certain degree of particle overlap (due to the finite thickness of the light sheet). When high-precision measurement of instantaneous individual particle positions (as opposed to coarse-grained mean velocity measurement) is needed, the light sheet is set to be as narrow as possible, and a high threshold of the peak intensity is selected so that only very sharp peaks (contributed by particles whose centers are precisely on the symmetrical plane of the light sheet) are admitted as valid data. The ultimate limit of precision in determining particle positions is set by the pixel width, corresponding to a few tenths of a particle diameter (depending on magnification.) All computations are performed using Interactive Data Language (IDL) programming.

We also analyze the spatial spectrum of each image slice. For instance, the horizontal spatial periodicity of a vertical image slice $\mathcal{I}_{slice}(x,z,t)$ can be represented by the following normalized Fourier spectrum averaged over depth z:

$$f(k_x,t) = \left\langle \frac{|F(k_x,z,t)|}{\left(\int |F(k_x,z,t)|^2 dk_x\right)^{1/2}} \right\rangle_z, \qquad (3)$$

in which $F(k_x,z,t) = \mathcal{F}_x[\mathcal{I}_{slice}(x,z,t)]$ stands for the Fourier transform in the x direction. The denominator is to correct the variation of image intensity over z and t. The intensity of a peak of this normalized spectrum $f(k_x,t)$ at a particular wave number $k_x^{(1)}$, corrected by subtraction of the background value, is defined as

$$I^{(1)}(t) = \frac{1}{2\epsilon}\int_{k_x^{(1)}-\epsilon}^{k_x^{(1)}+\epsilon} |f(k_x,t)|^2 dk_x - I_B^{(1)}(t), \qquad (4)$$

where $I_B^{(1)}(t)$ is a background value determined by averaging $|f|^2$ over a broader spectral interval centered at $k^{(1)}$ but excluding the wave numbers within $k_x^{(1)} \pm \epsilon$. When the wave number $k_x^{(1)}$ is chosen to match the mean horizontal spacing ($\approx 1d$) of particle centers in the crystallized state, the calculated peak intensity $I^{(1)}(t)$ can be used as an indicator of the growth of the crystalline order.

III. CRYSTALLIZATION TRANSITION

For a deep dense packing, long-term shearing by the upper boundary can induce a sharp change in the internal structure, accompanied by a significant decrease of granular volume and boundary shear force. The outcome is a crystallized state in which particles form horizontal hexagonally close-packed layers that move coherently in the flow direction, as we demonstrated in Ref. [42]. In this section, we characterize this process and its rheological consequences in detail, and describe the factors that influence the transition. In all of the experiments described below, if not specified otherwise, the annular channel contains 200 g of glass beads, which can create a 24-layer crystallized state.

A. Characterization of the transition

Simultaneous measurement of internal ordering, granular volume, shear force, and particle speed as functions of time are shown in Fig. 2. The disordered initial state is generally prepared by stirring the whole volume thoroughly. Time $t=0$ denotes the instant when the motion of the upper boundary begins to move at a speed of 12 particle diameters per second ($12d$/s); the bottom is flat.

In Fig. 2(a), the images show two instantaneous vertical slices at about one-third of the channel width from the outer vertical wall. They illustrate the disordered initial state ($t=0$) and the crystallized state ($t=60000$ s). A sample of the instantaneous spatial Fourier spectrum $f(k_x)$, defined in Sec. II, is shown in the inset. The intensity of its primary peak $I^{(1)}$ quantifies the degree of spatial order as a function of time. The displayed curve is smoothed over 20 frames (20 min in time) to reduce noise. The step rise of $I^{(1)}$ marks the occurrence of crystallization.

The change of the total granular volume is determined by measuring the vertical displacement of the upper boundary $h(t)-h(0)$ at fixed load, as shown in Fig. 2(b). The displacement, normalized by the mean height of the glass beads H_0, reveals a fractional change of total volume of about 3% at the crystallization transition. The absolute total volume can be computed from the geometrical parameters of the channel with an uncertainty primarily due to the rough boundaries, and the packing fraction of the final state is estimated as $(63\pm3)\%$. Meanwhile, the shear force as a function of time shows a simultaneous step decrease of about 15% at the crystallization transition, as shown in Fig. 2(c).

Figure 2(d) shows the local average of grain velocities in a region far below the sheared interface as a function of time. This is computed by averaging the velocities of particles in the region Γ indicated in the upper-right sample image, smoothed over 80 frames in time. The particles far below the sheared surface translate significantly more slowly after crys-

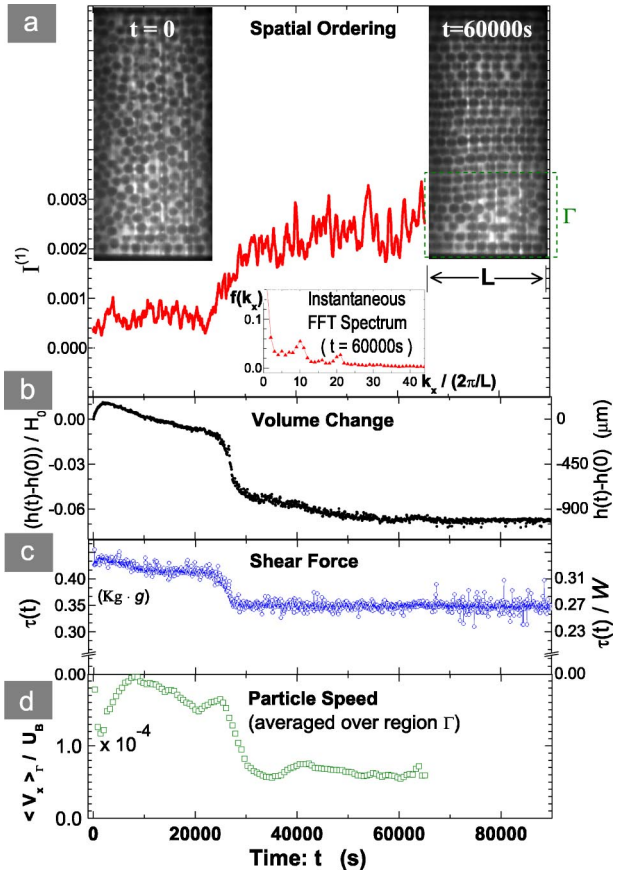

FIG. 2. (Color online) Simultaneous measurement of internal ordering, volume change, shear force, and particle speed as functions of time. Glass beads are driven at a speed of 12d per second from above. (a) Vertical image slices before and after the crystallization, with $I^{(1)}$ showing the intensity of the primary peak of the FFT spectrum, as are defined in Sec. II. (b) Fractional change of total height, as an indicator of total volume change. (c) Shear force, averaged once every rotation. (d) Particle speed averaged over the lower region Γ of the cell, as marked on the upper right image. The speed is normalized by the velocity of the driving boundary U_B.

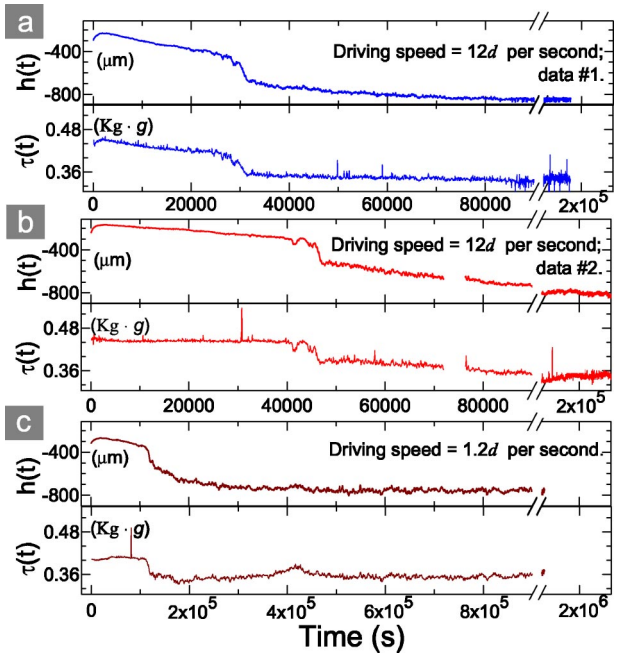

FIG. 3. (Color online) Sample histories of evolution as the upper boundary translates at constant speeds starting at $t=0$. The cell contains 200 g of glass beads with a flat bottom installed. In all cases, granular packings have been thoroughly stirred before $t=0$ but have not undergone boundary shearing. The changes of height of the upper boundary ht and shear force $\tau(t)$ are strongly correlated within each experiment. In cases (a), (b) and in Fig. 2, the glass beads are driven at exactly the same speed ($12d/s$), while the transition time exhibits stochastic variation. Case (c) is driven at a lower speed ($1.2d/s$). In all cases, the accumulated boundary translation at the time of the transition step is about 10^5d–10^6d in the direction of the flow.

tallization occurs, because the crystallized state has a stronger vertical decay of velocity (see Sec. V).

For a given driving speed and boundary condition, the time required for the disordered initial state to undergo a crystallization transition varies stochastically within about an order of magnitude, as shown by the records displayed in Figs. 2, 3(a), and 3(b). The time scale is consistent with the time required for the particles near the bottom to move a distance of several particle diameters relative to their neighbors or the bottom, and corresponds to about 10^5d–10^6d of accumulated translation of the upper boundary, where d is the particle diameter. The experiment shown as Fig. 3(c) is driven at $1/10$ of the typical driving speed, exhibiting the same features of transition at a later time, but within the same order of accumulated translation of the driving boundary.

Despite of the stochastic nature of the transition time, we note in Figs. 2 and 3 that the records of the total volume and shear force are strongly correlated in each experiment. The similarity is not limited to the time of the major transition step, but also many sub-features of the curves except those occasional spikes in shear-force records. (The occasional spikes are produced by brief isolated jamming events when smaller particles get caught in the gaps between the moving upper boundary and the stationary sidewalls.) These two boundary measurements, volume change and shear force, can both serve as sensitive indicators of the state of evolution. Figures 2 and 3 also show that a smooth initial dilation of granular volume can be detected within the first 10^4d of translation of the driving boundary; the exact amount of this dilation depends on the preparation of the initial state.

We have verified that the crystallization does not require a uniform speed of boundary translation, and is generic with or without interstitial fluid. In the absence of fluid [Fig. 5(b) in Ref. [42]], we find that the compaction steps also occur, but the accumulated translation of the driving boundary can be an order of magnitude longer than that for fluid-immersed particles under the same driving and boundary conditions. This suggests that friction plays a significant role in the underlying dynamics, and that this frictional interaction can be altered by the lubrication provided by the interstitial fluid.

B. Role of bottom condition

There are three different bottom boundary conditions that can be used for our experiments: (1) flat bottom, (2) mono-

layer bottom, and (3) bumpy bottom, as defined in Sec. II. The results show that the tendency to crystallize has a nonmonotonic dependence on the roughness of the bottom boundary. When we load the cell with 200 g of initially disordered glass beads and drive the upper boundary at the same speed ($12d/s$), a spontaneous transition to a 24-layer crystallized flow occurs when using either the flat or the monolayer bottom boundary (but not the bumpy boundary). Notably, experiments using the monolayer bottom [see the data presented in Ref. [42]] typically require less translation of the upper boundary to trigger the crystallization transition than those using the flat bottom. Furthermore, when less material is used, for instance 100 g of glass beads, a persistent 12-layer crystalline structure is quickly produced in experiments using the monolayer bottom boundary, while the flat-bottom experiment can only induce incomplete ordering that appears to be intermittent in the observation window. These observations demonstrate that the crystallization is produced most easily and completely using the monolayer boundary. The crystalline structure of the boundary, even if imperfect, appears to favor ordering in the bulk of the material, as occurs during epitaxial growth of ordinary solids.

In the case of the bumpy bottom, on the other hand, driving initially disordered glass beads for a long time gradually compacts the packing into a final state whose interior remains disordered indefinitely. Interestingly, the crystallization is then dependent on the history prior to the onset of the long-term unidirectional shearing, as we discuss in detail in Sec. IV. In all cases, the asymptotic values of granular volume consistently indicate the final state of internal order.

Although the bottom boundary condition can influence the crystallization of grains everywhere in the packing, different degrees of roughness of the boundary do not affect the interior velocity profiles (shown in Sec. V) measurably, once the same state of internal structure is created. Furthermore, regardless of the bottom boundary conditions, the asymptotic value of shear force for the disordered or crystallized final state is, respectively, equal to the typical value before or after the transitional step shown in Fig. 2(c). In other words, the mean shear force is sensitive to the internal packing structure, but not to the roughness of the bottom boundary.

C. Flows of different mean thickness

Using the monolayer bottom, which is the most favorable condition for complete crystallization, we compared the compaction histories of sheared flows for different amounts of glass beads in the channel [Fig. 5(a) of Ref. [42]], and found that the characteristic time for transition is diminished by two orders of magnitude when the total thickness of the material is halved.

Figure 4 demonstrates that the final thickness of the flow has a "quantized" dependence on the total mass M of the glass beads in the channel, corresponding to the creation of additional layers. This nonuniform increase of final thickness as M is increased can also be observed in thicker samples up to at least 24 layers thick. On the other hand, a smooth linear increase (not shown) is observed for comparable experiments using the bumpy bottom, for which the glass beads do not crystallize.

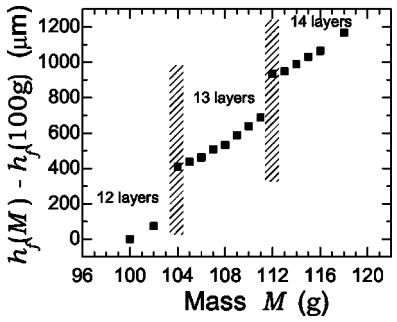

FIG. 4. Nonsmooth dependence of the final height $h_f(M)$ of the crystallized flows on the total amount (mass M) of glass beads. The height of the 100-g case is used as a reference. The monolayer boundary condition at the bottom is shared by all cases shown here. Specific numbers of well-defined ordered layers occur in discontinuous bands of M. The transition zones, in which crystallization is incomplete, are marked as shaded stripes.

It should be noted that the thinner flows exhibit incomplete crystallization at the transitional bands between adjacent zones, marked in Fig. 4 as the narrow shaded bands equivalent to about 1 g of total fill. As the total packing thickness is reduced to about six layers (50 g), these transitional bands can become as wide as 4 g, which is about half of the mass accounting for each layer on average. The wider the transitional bands, the easier it is to miss the crystallization phenomenon. This may explain why crystallization was not emphasized in previous experiments using thin layer flows to investigate shear band dynamics. On the other hand, the width of the transitional bands becomes undetectable in flows as thick as 24 layers, for which we find the transitional band to be less than $1/8$ of the mass of one layer.

D. Discussion

The simultaneous step decrease at the crystallization transition of volume, shear force, and grain speed (in the lower part of the sample volume) indicates that the crystallized state transfers horizontal momentum downward less efficiently than does the disordered state, even though the crystallized state is denser. This observation demonstrates that granular density alone does not determine the rheology of the material.

A bumpy bottom boundary is sufficient to suppress the shear-induced crystallization everywhere in the deep random packing equivalent to 24 layers of grains. A monolayer bottom is found to be the preferred boundary condition to complete the crystallization process. This fact may be attributed to the spatial periodicity of the monolayer packing. A scenario similar to epitaxial growth [28,44] with the lower boundary playing the role of template seems plausible in view of the sensitivity to bottom conditions, the observed timescale of the transition, the stochasticity of the required time, and its drastic change with mean layer thickness. However, the ordering is inhomogeneous: the degree of order visible in a particular slice of the whole annular channel appears intermittent and often nonuniform during the transition. There is no clear evidence that the crystallization grows from the bottom upwards.

Our mean packing fraction in the crystallized state $(63\pm3)\%$ is lower than the theoretical value for a hexagonal close packing ($\pi/\sqrt{18}\approx74\%$), because the extra space and defects are necessary to allow the flow and to accommodate the circular finite-sized container. On the other hand, the mean density of the crystallized state here is close to but slightly higher than $\sqrt{3}\pi/9\approx60\%$, which is the theoretical value for parallel planes of hexagonally packed particles with a spacing exactly equal to the particle diameter. Presumably the actual value is affected by the degree of overlaps or interpenetration of adjacent layers, and the density of defects. The packing fraction of the disordered initial state is roughly 3% less, significantly lower than the reported values for random close packing [43]; in our experiments, even the crystallized state is not denser than the conventional random close packing.

IV. NONUNIQUE SELECTION OF FINAL STATES

When using a sufficiently bumpy bottom boundary (described in Sec. III B), we find that the final state is not unique. Whether the interior of the dense packing evolves into a crystallized or a disordered final state as a consequence of the unidirectional driving of the monolayer upper boundary depends on the prior history. In particular, applying a few initial cycles of oscillatory shear can significantly alter the evolution.

We first describe in Sec. IV A the basic phenomena that occur when granular material is subjected to oscillatory driving. Then, in Sec. IV B, we show that an initial oscillatory shear, if applied prior to a long-term unidirectional shearing, can induce crystallization in a situation where it would otherwise not occur.

A. Behavior during temporary oscillatory shear

Following a long-term unidirectional shearing, we alternate the direction of upper boundary a few times, traveling 10^2d each way, as illustrated in Fig. 5(a). Meanwhile, the height of the upper boundary is measured at the midpoint of its travel in either direction. The data show the compaction in response to the oscillatory shear. The right half of Fig. 5(a) shows that, for both crystallized and disordered states that have undergone a long-term unidirectional shear before applying the alternating driving (as many as 60 reversals), the glass beads recover their original volume as the unidirectional driving resumes, with their internal ordering remaining unchanged (as evidenced by simultaneous internal imaging, not shown).

At each starting point of the boundary motion in the opposite direction, an excess internal motion of grains can be observed as shown in Fig. 5(b). The sudden motion of grains by a distance of the order of $d/2$ is found to be generic to both crystallized and disordered states. The excess internal motion is absent if the boundary driving is restarted in the same direction as that of its previous stage; this is illustrated by the absence of the spike upon the first step change of boundary speed in the graph (time step 25). Signs of excess grain motion similar to the phenomena reported here have also been observed in the surface flow of grains in a Coutte geometry upon reversal of shearing, as reported in a previous study [51].

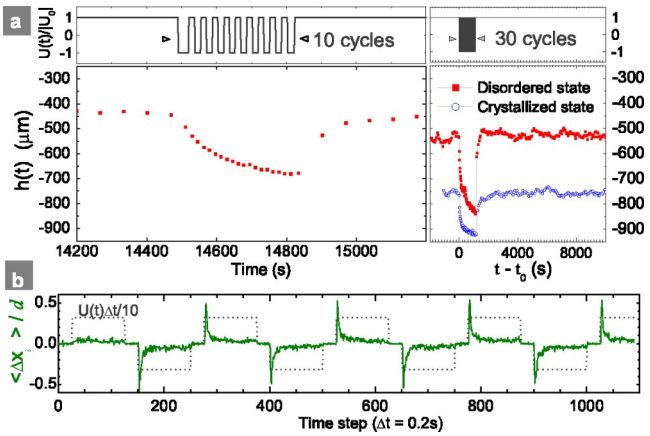

FIG. 5. (Color online) Compaction and internal grain motion in response to temporary oscillatory driving. (a) Boundary velocity $U(t)$ and the response of $h(t)$, the time-dependent height of the granular packing. The upper boundary moves at a speed $|U_0|=12d$ per second in its steady state. Three records share the same boundary condition and reference height, and therefore can be compared. Time axes for the two records on the right are shifted horizontally for display purpose, with t_0 labeling the start of the oscillatory shearing. (b) Ensemble-averaged displacements of internal grains sampled every 0.2 s. Displacements are averaged over roughly 60 grains at the midheight of a disordered packing. The time-dependent driving velocity $U(t)$ is overlaid on the data to indicate the phase of boundary motion. Note the spike upon each reversal of the driving velocity $U(t)$.

Accompanying the brief excess motion, a sudden drop of the upper boundary of about $d/5$ can be detected, although it is not reflected in Fig. 5(a) due to the discrete sampling. The right-hand side of Fig. 5(a) also shows the responses of disordered and crystallized states created under the same boundary conditions (described in Sec. IV B), and indicates that the total volume of the disordered state can temporarily become smaller than the steady volume of the crystallized state. These facts suggest that the compaction induced by oscillatory shear is highly nonuniform over the depth, and is perhaps primarily due to rearrangement of grains near the upper boundary. Therefore, one should be aware that the total volume does not instantaneously reflect the state of material deep in the interior. On the other hand, translating the upper boundary for a distance of about 10^3d is sufficient for the material to recover its volume prior to the temporary unsteady driving; therefore, the total volume can still serve as an indicator of internal state of a steadily sheared flow, as long as a possible delay of response is taken into account.

B. Stochastic outcomes of unidirectional shearing combined with oscillatory pretreatment

When a few oscillatory cycles [as in Fig. 5(a)] are applied just after the random packing is prepared by thoroughly stirring the entire volume, subsequently applying a sustained unidirectional shear can lead to either a crystallized final

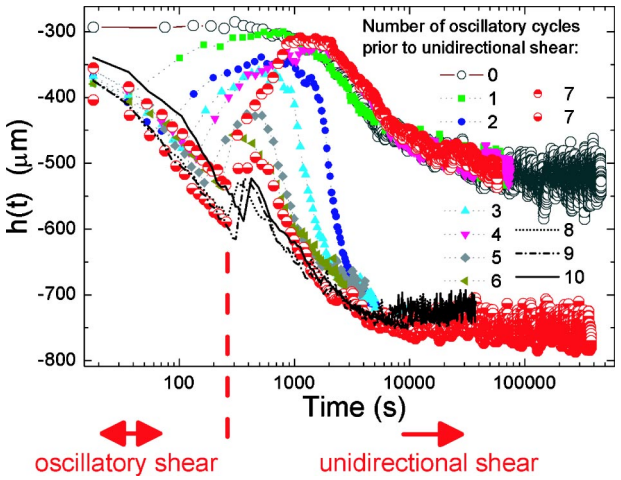

FIG. 6. (Color online) Nonunique selection of final states, indicated by the long-term evolution of the packing height $h(t)$. With only unidirectional shearing (labeled empty circles), the system always approaches a disordered final state (joining curves at the top right). On the other hand, applying a few cycles of oscillatory shearing to the uncompacted packing causes the system to evolve stochastically into either a disordered state, or a denser crystallized state (joining curves at the bottom right).

state or another final state that remains disordered in its interior. This is demonstrated by Fig. 6, where the volume compaction is used as an indicator of the long-term evolution. The route of the evolution appears stochastic, as the same number of cycles of oscillatory pretreatment can lead to different final results, although a large number of oscillatory cycles tends to produce a crystallized final state. But without the oscillatory pretreatment, applying a unidirectional shearing alone over a long time will not produce a crystallized state with a bumpy bottom boundary. Evidence from simultaneously recording the internal images shows that a large number of oscillatory cycles causes grains to organize into clearly identifiable layers in the upper half of the layer. The spatial ordering in the field of view during the subsequent unidirectional shearing can appear intermittent; this observation suggests that the ordering induced by oscillatory shear is inhomogeneous.

C. Shear-induced stabilization of the disordered state

It is remarkable that, if the oscillatory cycles (as illustrated in Sec. V) are applied after the material has experienced a long-term unidirectional shearing, then the oscillatory treatment becomes ineffective in producing internal order: even though oscillatory driving still causes the upper boundary to descend as shown in Fig. 5(a), simultaneous internal imaging reveals that the system shows no sign of partial ordering after as many as 60 reversals of boundary motion have been applied. Also Fig. 5(a) shows a quick recovery after the unidirectional shearing is resumed. These facts suggest that the oscillatory boundary driving does not change the deep interior of a sufficiently compacted packing significantly. Further experiments suggest that prolonged unidirectional shearing of a dense packing can eliminate this "extra" interparticle space which would otherwise allow the sudden jump of grains upon the reversal of the boundary motion as shown in Fig. 5(b); this phenomenon will be reported subsequently [45].

On the other hand, a crystallized state is always stable against oscillatory boundary shearing; the ordered structure can only be destroyed by stirring the packing manually.

D. Discussion

We have found that, for given driving and boundary conditions (a long-term unidirectional shearing and a bumpy bottom), the final state of a continuously driven flow can be nonunique. The selection of a crystallized or a disordered final state partly depends on the preparation history prior to the long-term shearing, and can appear stochastic if the material has not been sufficiently compacted by unidirectional shear. In comparison to unidirectional shearing, oscillatory driving is more effective in producing the partial order that generally favors the evolution towards a crystallized final state. This effectiveness may be related to the extra flexibility of the packing toward rearrangements when the shear stress is briefly relieved upon each reversal of the boundary motion, as suggested by the excess internal motion shown in Fig. 5(a). In addition, the quasihexagonal structure of the monolayer driving boundary may in part account for creation of this partial ordering.

Evidence from time series of internal images suggests that the the partial ordering induced by the oscillatory pretreatment is inhomogeneous. In the subsequent unidirectional shearing, whether the system selects the route of a global crystallization or a complete elimination of the crystalline order may depend on the extent and spatial distribution of this partial ordering. This is perhaps the reason why the outcomes of the subsequent shear-induced evolution of internal structure appears stochastic.

Both the crystallized state and disordered state can be stable against oscillatory boundary motion, after being sufficiently compacted by a unidirectional shear. On the other hand, we also recognize that the reverse of a crystallization transition never occurs unless we reset the system by stirring the packing manually. A tentative explanation is that the crystallized state is less dissipative and is therefore a "preferred" state of flow compared to the disordered state.

Our observation that unidirectional shearing gradually stabilizes a disordered state demonstrates that substantial change in the properties of a granular packing can slowly occur as a result of a long-term evolution. This change is a type of smooth evolution that is different from the sharp distinctive change of internal structure exemplified by the crystallization process. It is important that any successful model for dense granular flow be able to account for both types of evolution under long-term shearing.

As a possible theoretical approach to understanding the phenomena described in this section, one might regard the crystallized and disordered states as attractors in a space-time dynamical system. The structure of the phase space and its attractors would be affected by variables such as the total volume and the boundary conditions. For example, for the

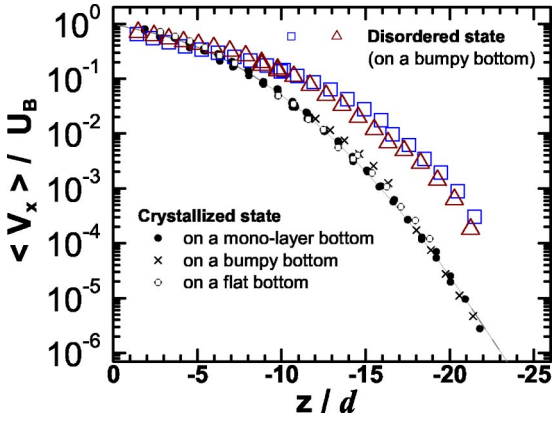

FIG. 7. (Color online) The asymptotic mean velocity profiles for different final states and boundary conditions. Velocities are normalized by the speed of the driving boundary, which is close to $z=0$. The positions of the top layer (indicated by the left endpoint of each data set) are slightly different for flows of different final states or on different bottom conditions, but are within the order of grain diameter. The data points for the crystallized state on the monolayer bottom are fitted by a quadratic curve shown in gray. (The triangles and squares represent disordered-state velocity profiles measured during the same experiment but at two different vertical planes. The distance from each of the two vertical plane to the outer sidewall are, respectively, 1/4 and 1/3 of the spacing between the concentric cylindrical walls.)

flat or monolayer bottom boundary, there is only a single attractor (the ordered state), while for the bumpy bottom, there are two attractors. The role of the oscillatory shearing could perhaps be modeled as a perturbation affecting the current position of the system point relative to the attractor(s). It would be interesting to consider how to define the variables spanning phase space and the underlying differential equations to implement such a "dynamical systems" explanation.

V. VELOCITY PROFILES OF THE TWO FINAL STATES

In Fig. 7, we compare the time-averaged particle velocity of different final states measured along vertical image slices. For either the crystallized or the disordered state, the sampling starts after the packing has evolved under an unidirectional shearing at a speed of $12d/\mathrm{s}$ for several days, corresponding to $10^6 d$ of total translation of the upper boundary. This ensures that the velocity field has reached the asymptotic value. Since the height-dependent grain velocity varies over several decades, we extract particle velocities from local imaging of patches recorded at different frame rates (as illustrated in Fig. 2 of Ref. [42]); each data point is determined from a local average over $10^2 d$ of accumulated particle displacement. Within the entire range of parameters used in our experiments, the local mean velocity varies smoothly with vertical position; we do not observe abrupt internal shear zones such as those reported in previous simulations of sheared dense packings with a large imposed pressure [8] or of dilute repulsive particles under suitable conditions [21].

For the 24-layer crystallized state, the data marks in Fig. 7 also indicate the mean positions of each well-defined layer, relative to a common reference height approximately at the driving boundary. It can be deduced from the slope on this semilog plot that the exponential decay length gradually varies from approximately $5d$ on the top, to $1d$ near the bottom. For the disordered final state created with the same amount of glass beads, the height-dependent asymptotic velocity are measured at two vertical planes during one experiment. This is because, unlike the crystallized state, the grain velocity of a disordered state shows a decay towards the sidewalls [42,45] although generally not more than a factor of 10; there exists a finite slip velocity against the sidewalls. Velocity profiles of either state obtained from multiple experiments (reset by fully stirring the grains) can differ slightly; maximal variation found near the bottom of the flow but is still less than a factor of 10. This variation may be related to small differences in the degree of local ordering in the lower portion of the flow, which evolves rather slowly. Information regarding the reproducibility of the velocity profiles and the calibration methods that are used for combining different image patches will be provided in a forthcoming thesis [46].

Our measurements show that the downward decay of the asymptotic mean velocity in the crystallized state is significantly steeper than in the disordered state. A similar effect is also qualitatively reflected in the step decreases of lower-layer particle velocity at the crystallization transition as shown in Fig. 2(d), even though the grain velocity in the disordered phase may not have reached its asymptotic profile before the transition occurs. A plausible explanation is that the stronger decay of velocity in the crystalline state is a consequence of the reduction of downward transfer of horizontal momentum due to the formation of hexagonally ordered horizontal sheets (Fig. 4 of Ref. [42]) that slip over adjacent layers in a coherent way that generates less shear resistance than in a disordered state; this is consistent with the direct measurement of shear force. In addition, we investigate the individual and collective particle motion in the macroscopically steady states, as well as during the transient response; several interesting phenomena, such as the behavior similar to the zigzag motion discussed in Refs. [21,25], will be reported in a subsequent publication [45].

Internal imaging of the generally disordered state reveals that grains near the sidewalls can become locally ordered in vertical planes with local hexagonal structure. This wall-induced local order is oriented quite differently than the horizontal planes of the globally crystallized state. For example, in the images for calculating the disordered-state velocity profiles in Fig. 7, this hexagonal structure is visible at one vertical plane that is closer to the sidewall than the other plane, in which grain configuration appears to be random. In Fig. 7, we choose the bin width for the disordered state in a way that each of the triangles corresponds to one row in the 22-layer sidewall-induced structure. Nevertheless, the presence of this sidewall-induced local order does not have as strong an impact on the velocity profile as does the 24-layer structure of the crystallized state, because the sidewall-induced structure is not oriented in a way that favors slip between layers oriented perpendicularly to the imposed velocity gradient. This is a useful example showing that the

local granular rheology depends not only on degree of ordering, but also on its orientation.

The increased spatial gradient of the particle velocity in the crystallized state, and the observed step decrease of granular volume and shear force (Fig. 2), suggest an interpretation of the crystallization transition as producing an anomalous reduction of local "viscosity" at all depths, despite the larger coarse-grained density in the crystalline state. However, the concept of viscosity in ordinary fluid mechanics is questionable in the present context, because the numerical value of the local viscosity would have an anomalously wide distribution for two reasons: (1) The local velocity gradient varies drastically with depth, while conservation of momentum suggests the shear stress does not change by the same amount unless the drag force exerted by the sidewalls is very large—a very unlikely scenario in our apparatus with the aspect ratio of cross section in order one as well as the smoothness of sidewalls. (2) The steady-state shear force in our system does not show measurable dependence on driving speeds, and can persist almost indefinitely after the stepping motor is turned off, showing no detectable change beyond the span of our observation (more than a week). The extremely slow relaxation of stress in dense granular materials is discussed in a previous work by Hartley and Behringer [47].

The velocity profile of the crystallized state can be fitted to a quadratic curve on the semilog graph and gives $V_x(z)/U_B = 0.798 \exp\{0.103[(z-z_0)/d] - 0.02375[(z-z_0)/d]^2\}$, where the reference height $z_0 = -1.3d$ is the height of the interface between the driving surface and the grains as observed from the images. The decay length can be exacted by defining $l(z) = V_x(z)/V_x'(z)$. The range of values of $l(z)/d$ observed here are generally larger than the measurements in Refs. [30,32], but smaller than some two-dimensional simulation results [8,16]. A full discussion of the functional form of the velocity decay, its dependence on the total thickness of the flow and particle size, and the comparison of our measurements with previous work on the velocity profile, are beyond the scope of this paper and will be included in a separate publication [45].

VI. CONCLUSION

Granular packings driven by a slowly moving boundary exhibit complex time evolution of internal structure and rheology. For a thick packing of nearly mono-disperse granular material under long-term unidirectional shearing, the final outcomes can be categorized into two well-defined states: (1) A crystallized state in the form of creeping hexagonal lattice planes oriented perpendicularly to the imposed velocity gradient; the structure is global and persistent, but contains some defects; (2) a disordered state in which no significant spatial order is found in the bulk, except in a few layers near the smooth vertical confining walls. When the system is driven under a fixed normal load, the granular packing undergoes a decrease of total volume with time before settling into either of the two final states. Once sufficiently compacted, both states are stable against perturbations produced by oscillatory shearing.

The different internal packing structures result in significant differences in the rheology of these two states. The time-averaged particle velocity fields differ qualitatively [42,45]. In the crystallized case, the particles form nearly rigid planar structures that are parallel to the driving boundary while translating with different mean speeds; the coherence length for each plane spans the entire system (about 30 grain diameters horizontally). The disordered state, on the other hand, exhibits significant decay of grain velocity towards the smooth concentric sidewalls. Our precision measurements of the height-dependent time-averaged grain velocity, which span more than five decades, indicate that the velocity in the crystallized state declines more rapidly with depth than occurs in the disordered state. In addition, both the granular volume and the boundary shear force are significantly less in the crystallized state than in the disordered state; therefore these two external measurements can serve as alternative indicators of the state of the interior when direct internal imaging is not available (e.g., in systems of dry grains).

The stronger gradient of velocity and smaller resisting shear force in the crystallized state (compared to the disordered state at the same normal load and driving speed) can be consistently explained: the hexagonally ordered layers can slip over each other coherently; this results in a lower resistive force and a stronger reduction of mean velocity with distance from the driving boundary.

The scenario of the evolution and stability of the two states of internal order under shear driving depends on both the boundary condition of the stationary substrate and the density of the initial packing. When a thick granular packing is placed on a bumpy stationary substrate, an uncompacted disordered state can be unstable in the sense that a few cycles of oscillatory driving can promptly generate significant partial ordering in the bulk. Driven by a unidirectional shearing subsequently, this partial ordering can either be eliminated or can evolve into a global crystallization in an apparently stochastic fashion, depending on details of the partially ordered state. On the other hand, once the disordered state with the same boundary conditions has been sufficiently compacted, e.g., by a long-term unidirectional shearing with a fixed normal load, the disordered state becomes highly stable; oscillatory shearing becomes ineffective in generating the partial ordering that can be induced in the uncompacted case.

On the other hand, when we use either a flat substrate or monolayer bottom with a quasihexagonal structure (which appears to be the most favorable boundary condition for crystallization), the disordered state is generally unstable against boundary shearing and always evolves into a globally crystallized state. When a unidirectional boundary shearing is applied to a thick packing with these substrate conditions, the crystallization transition occurs with a long precursor in which internal grains remain largely disordered; compared to the entire course of evolution, the crystallization transition appears as a relatively sharp change where granular volume, the shear resistance, and the grain velocity profile simultaneously change, along with the degree of internal ordering. The duration of the precursor appears stochastic within an order of magnitude, and is comparable to the characteristic time for the grains near the stationary bottom to move a few

particle diameters relative to the boundary, or to each other; this characteristic time varies drastically with the thickness of the packing and scales inversely with the driving speed. The sensitivity to substrate conditions and the long precursor seems to imply a mechanism similar to epitaxial growth [44,28]. However, there is no clear evidence that the ordered domain grows from the substrate upwards, because the observed crystallization process is highly nonuniform. In any case, the abrupt appearance of the shear-induced crystallization of an initially disordered state may be unique to granular flows due to their strongly nonlinear velocity profile, in contrast to other sheared flows such as colloidal suspensions.

For granular packings with smaller total thickness, for example, 14 equivalent layers or less, the crystallization can be incomplete and shows a quantized dependence on the exact amount of material in the system. As the total thickness decreases, the "two states" as well as their stability become less well defined. For these reasons, our discussions above focus on sheared granular packings as thick as 24 equivalent layers. Detailed information regarding the grain-level dynamics of internal grains, including their time evolution and response to unsteady driving, will be provided in a subsequent publication. Further experiments are needed to understand other factors that influence the time evolution of packed granular material under shear, for instance, the role of particle anisotropy or polydispersity, which leads to size segregation and should suppress crystallization.

The granular flow reported here is in the creeping (quasistatic) regime throughout the entire system. This is not only suggested by theoretical estimates, but is also consistent with experimental facts. For instance, the measured velocity varies smoothly with position, and has a functional form that is invariant with respect to two decades of change in driving speeds [42]. The magnitude of time-averaged grain velocity at each height scales linearly with the imposed boundary speed, down to extremely slow boundary translation $(0.1d/s)$.

This work on creeping flows raises interesting theoretical questions: how to relate the granular rheology to the internal structure; how to explain the ordering mechanisms under steady or oscillatory driving; how to construct a model with a minimal set of internal state variables to account for the stability of different internal structures, the apparent stochastic selection of evolution, and the gradual compaction-induced stabilization. In Sec. IV D, we speculated about the possibility of constructing a dynamical systems picture of the state of order of the system.

The connection between creeping flow and granular static states [48] is also interesting: given the observed irreversible evolution over time, our observations raise the question of whether a slowly creeping flow can be viewed as a stationary ergodic ensemble of all possible static particle configurations (as is commonly assumed, for instance, in Ref. [31]). It may instead be a weighted subset in which some configurations of particles become inaccessible as the total volume evolves. To understand the gradual evolution of slowly flowing granular materials, further development of experimental probes into the evolving internal structure, supplemented by noninvasive detection of interparticle stress (see, e.g., Ref. [49]), seems highly desirable.

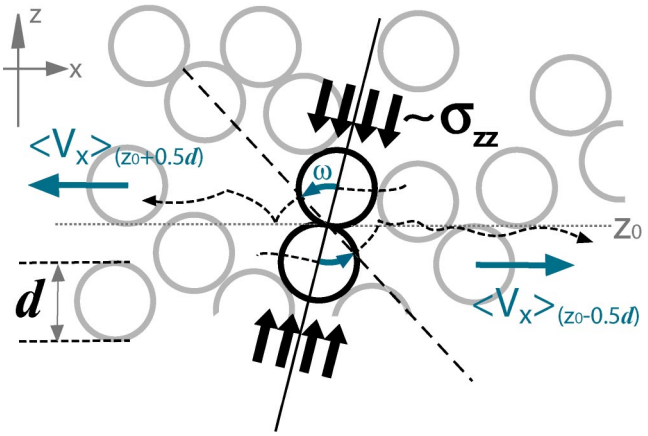

FIG. 8. (Color online) Schematic representation of a granular shear flow. Two highlighted spheres are in contact at height z_0. The dashed curves represent the center-of-mass trajectories of each sphere.

ACKNOWLEDGMENTS

We appreciate the contributions of Tom Lubensky and Greg Voth to this work. We thank Baruch Meerson and Mark Robbins for sharing with us information regarding the computer simulations performed in their research groups. J.C.T. is grateful to Bruce Boyes for his assistance in constructing the apparatus. This work is supported by the NSF Division of Materials Research under Grants No. DMR-0072203 to Haverford College, and DMR-0079909 to the University of Pennsylvania (J.C.T.).

APPENDIX: RANGE OF DRIVING SPEEDS TO PRODUCE CREEPING FLOWS

Here we estimate the upper bound of driving speeds for a sheared dense packing to remain in the regime of creeping (quasistatic) flow, under a fixed normal load. Consider uniformly sized, noncohesive, rigid particles of mass m and diameter d, packed under a compressive load along z and sheared along $+x$ and $-x$, as shown in Fig. 8. Here we choose a local reference frame in which the value of time-averaged velocity $\langle V_x \rangle$ as a function of height z appears antisymmetric with respect to z_0, a reference height where the two highlighted particles contact. If the local granular stress is high enough to keep all contacting particles in either static or sliding contact for a finite duration (until they are eventually pulled apart), these two particles would move around the contact point with a radius of curvature $d/2$ and an angular velocity $\omega \approx \langle V_x \rangle_{z_0+0.5d}/0.5d \equiv \dot{\gamma}$. Because the assumed noncohesive contacts between the two spheres only sustain a positive stress but not a tension, this is equivalent to the condition that the "normal" component (F_N) of the total force exerted by all surrounding particles on each of the two highlighted spheres needs to be greater than the centripetal force $m\omega^2 d/2$ required for the local circular motion. That is,

$$m\dot{\gamma}^2 d/2 \approx m\omega^2 d/2 < F_N \approx \sigma_{zz} d^2, \tag{A1}$$

in which σ_{zz} stands for coarse-grained normal stress along the z direction. We can define a dimensionless number

$X \equiv \frac{1}{2} m \dot{\gamma}^2 d^{-1} \sigma_{zz}^{-1}$, which represents the ratio of the centripetal force per particle to the normal force per area d^2. The stress component σ_{zz} can either be mechanically imposed, or arise from grain's self-weight, or both. We can alternatively express $\sigma_{zz} d^2$ as mgN_{eq}, in which N_{eq} is the equivalent number of layers whose weight produces a stress σ_{zz} at the location being considered. For granular materials in a sufficiently wide container where the Janssen effect can be neglected [4], grain weight contributes to the normal stress at any horizontal internal plane with the corresponding N_{eq} equal to the actual number of layers packed above the plane considered.

The shear rate $\dot{\gamma}$ can be approximated by $\langle V_x \rangle / l$ where l is the local exponential decay length for grain velocity, with l having empirical values of a few particle diameters. For a packing sheared from above under the influence of gravity, the highest shear rate $\dot{\gamma}$ and lowest stress σ_{zz} occur at the first layer adjacent to the shearing surface; therefore the criterion Eq. (A1) becomes

$$m\left(\frac{U_0}{l}\right)^2 d/2 < \sigma_{zz} d^2 \tag{A2}$$

or alternatively

$$m\left(\frac{U_0}{l}\right)^2 d/2 < mgN_{eq}, \tag{A3}$$

where U_0 stands for the mean velocity of the first layer, which is close to the boundary speed. Using the parameters $d = 10^{-1}$ cm, $N_{eq} = 10^2$, $g = 10^3$ cm/s^2 and an empirical value $l = 3d$, we estimate that the transition threshold for U_0 is $4 \times 10^3 d$/s, which is more than two orders of magnitude higher than the highest driving speed $12d$/s used in our experiments. Therefore, the shear flows reported in this paper are entirely in the creeping (quasistatic) regime where $X \ll 1$.

When the shear rate $\dot{\gamma}$ is high or the stress is low, it is possible to reverse the inequalities above; for example, transition from the regime of creeping flow into the "granular gas" regime can be found either locally or globally in high-speed annular shear cells [35,37] with their normal load reduced by a counterweight. For an inclined gravity-driven granular flow with an upper free surface, it is commonly observed that particles within a few grain diameters of the surface are in a dynamical regime that is qualitatively different from that of the creeping grains deep down. (See the experiments and measured velocity profiles in Refs. [30,50].) Note that with an upper free surface, the smallest meaningful value of N_{eq} in the estimate proposed here should be 1 instead of 0, due to the weight of the first layer itself.

In the preceding discussion, cohesivity, friction, finite rigidity (elasticity) of grains, and their interaction with interstitial fluids are neglected; the analysis here is meant to be an order-of-magnitude estimate of the threshold above which the departure from creeping flow can occur.

[1] R. Behringer, H. Jaeger, and S. Nagel, Chaos **9**, 509 (1999).
[2] E. Clement, Curr. Opin. Colloid Interface Sci. **4**, 294 (1999).
[3] I. Goldhirsch, Annu. Rev. Fluid Mech. **35**, 267 (2003).
[4] R. M. Nedderman, *Statics and Kinematics of Granular Materials* (Cambridge University Press, Cambridge, 1992).
[5] M. Moakher, T. Shinbrot, and F. J. Muzzio, Powder Technol. **109**, 58 (2000).
[6] J. M. Ottino and D. V. Khakhar, Powder Technol. **121**, 117 (2001).
[7] G. Mandl, *Mechanics of Tectonic Faulting: Models and Basic Concepts* (Elsevier, Amsterdam, 1988).
[8] E. Aharonov and D. Sparks, Phys. Rev. E **65**, 051302 (2002).
[9] L. Kondic and R. Behringer, e-print cond-mat/0307555.
[10] C. S. Campbell, J. Fluid Mech. **465**, 261 (2002).
[11] I. S. Aranson and L. S. Tsimring, Phys. Rev. E **65**, 061303 (2002).
[12] G. Debregeas and C. Josserand, Europhys. Lett. **52**, 137 (2000).
[13] D. Kolymbars, *Constitutive Modelling of Granular Materials* (Springer, Berlin, 2000).
[14] L. S. Mohan, K. K. Rao, and P. R. Nott, J. Fluid Mech. **457**, 377 (2002).
[15] S. B. Savage, J. Fluid Mech. **377**, 1 (1998).
[16] D. Volfson, L. S. Tsimring, and I. S. Aranson, Phys. Rev. E **68**, 021301 (2003).
[17] D. Z. Zhang and R. M. Rauenzahn, J. Rheol. **41**, 1275 (1997).
[18] A. Sierou and J. F. Brady, J. Rheol. **46**, 1031 (2002).
[19] J. J. Erpenbeck, Phys. Rev. Lett. **52**, 1333 (1984).
[20] J. F. Lutsko, Phys. Rev. Lett. **77**, 2225 (1996).
[21] M. J. Stevens and M. O. Robbins, Phys. Rev. E **48**, 3778 (1993).
[22] S. Butler and P. Harrowell, Phys. Rev. E **52**, 6424 (1995).
[23] J. Delhommelle, J. Petravic, and D. J. Evans, Phys. Rev. E **68**, 031201 (2003).
[24] P. Chaikin *et al.*, in *Physics of Complex and Supermolecular Fluids* (Wiley-Interscience, New York, 1987), p.65.
[25] S. E. Paulin, B. J. Ackerson, and M. S. Wolfe, Phys. Rev. E **55**, 5812 (1997).
[26] M. D. Haw *et al.*, Phys. Rev. E **58**, 4673 (1998).
[27] O. Pouliquen, M. Nicolas, and P. D. Weidman, Phys. Rev. Lett. **79**, 3640 (1997).
[28] Y. Nahmad-Molinari and J. C. Ruiz-Suarez, Phys. Rev. Lett. **89**, 264302 (2002).
[29] L. E. Silbert, G. S. Grest, S. J. Plimpton, and D. Levine, Phys. Fluids **14**, 2637 (2002).
[30] T. S. Komatsu, S. Inagaki, N. Nakagawa, and S. Nasuno, Phys. Rev. Lett. **86**, 1757 (2001).
[31] B. Miller, C. Ohern, and R. P. Behringer, Phys. Rev. Lett. **77**, 3110 (1996).
[32] D. M. Mueth *et al.*, Nature (London) **406**, 385 (2000).
[33] D. M. Mueth, Phys. Rev. E **67**, 011304 (2003).
[34] L. Bocquet *et al.*, Phys. Rev. E **65**, 011307 (2002).
[35] D. M. Hanes and D. L. Inman, J. Fluid Mech. **150**, 357 (1985).
[36] S. B. Savage and M. Sayed, J. Fluid Mech. **142**, 391 (1984).
[37] S. S. Hsiau and W. L. Yang, Phys. Fluids **14**, 612 (2002).
[38] F. Dalton and D. Corcoran, Phys. Rev. E **63**, 061312 (2001).

[39] W. H. Press, S. A. Teukolsky, W. T. Vetterling, and B. P. Flannery, *Numerical Recipes in C: The Art of Scientific Computing*, 2nd ed. (Cambridge University Press, Cambridge, 1992).
[40] J. C. Crocker, Ph.D. thesis, University of Chicago, Chicago, 1996.
[41] D. H. Ballard and C. M. Brown, *Computer Vision* (Prentice-Hall, Englewood Cliffs, NJ, 1982.).
[42] J.-C. Tsai, G. A. Voth, and J. P. Gollub, Phys. Rev. Lett. **91**, 064301 (2003).
[43] S. Torquato, T. M. Truskett, and P. G. Debenedetti, Phys. Rev. Lett. **84**, 2064 (2000).
[44] J. P. Hoogenboom *et al.*, Phys. Rev. Lett. **89**, 256104 (2002).
[45] J.-C. Tsai and J. P. Gollub (in preparation).
[46] J.-C. Tsai, Ph.D thesis, University of Pennsylvania, Philadelphia, 2004.
[47] R. R. Hartley and R. P. Behringer, Nature (London) **421**, 928 (2003)
[48] S. F. Edwards and D. V. Grinev, Adv. Phys. **51**, 1669 (2002).
[49] D. W. Howell, R. P. Behringer, and C. T. Veje, Chaos **9**, 559 (1999).
[50] N. Taberlet *et al.*, Phys. Rev. Lett. **91**, 264301 (2003).
[51] W. Losert and G. Kwon, Adv. Complex Syst. **4**, 369 (2001)